Journal of Solid State Chemistry 325 (2023) 124170

Contents lists available at ScienceDirect

Journal of Solid State Chemistry

journal homepage: www.elsevier.com/locate/jssc

High-pressure synthesis, crystal structure, and characterization of the new non-centrosymmetric terbium borate $Tb_3B_{10}O_{17}(OH)_5$

Tobias A. Teichtmeister [a], Christian Paulsen [b], Sebastian J. Ambach [c], Klaus Wurst [a], Lkhamsuren Bayarjargal [d], Wolfgang Schnick [c], Hubert Huppertz [a,*]

[a] Institut für Allgemeine, Anorganische und Theoretische Chemie, Universität Innsbruck, Innrain 80–82, 6020, Innsbruck, Austria
[b] Institut für Anorganische und Analytische Chemie, WWU Münster, Corrensstraße 30, D-48119, Münster, Germany
[c] Department of Chemistry, Ludwig-Maximilians-University Munich, Butenandtstraße 5-13, D-81377, Munich, Germany
[d] Institut für Geowissenschaften, Abt. Kristallographie/Mineralogie, Goethe-Universität, Altenhöferallee 1, D-60438, Frankfurt am Main, Germany

ARTICLE INFO

Keywords:
Crystal structure
High-pressure
Multianvil
Rare-earth borate
Terbium

ABSTRACT

Herein, the high-pressure/high-temperature synthesis (11 GPa, 650 °C) of $Tb_3B_{10}O_{17}(OH)_5$ in a modified Walker-type multianvil device is presented. The structure of this rare-earth borate was determined by single-crystal X-ray diffraction methods and was found to crystallize orthorhombically in the space group $Pmn2_1$ (no. 31) with the unit cell parameters a = 16.2527(4), b = 4.4373(1), and c = 8.8174(2) Å. The new compound was further characterized using infrared spectroscopy, energy-dispersive X-ray spectroscopy, second harmonic generation (SHG) measurements, and temperature-dependent X-ray powder diffraction. $Tb_3B_{10}O_{17}(OH)_5$ decomposes to β-$Tb(BO_2)_3$ at temperatures higher than 460 °C. With increasing temperatures, the formation of μ-$TbBO_3$ was observed, which transforms to π-$TbBO_3$ upon cooling.

1. Introduction

Borates are of great industrial and academic interest. While their excellent optical properties combined with great chemical stability make them interesting materials for e.g. non-linear optical applications, their structural diversity is unmatched among other substance classes and thus supports their role as a great model system for structure-property-relationship studies [1,2]. Hitherto, several terbium ortho- and metaborates [3–7], the high-pressure phase α-$Tb_2B_4O_9$ [8], and one hydroxyl-containing compound $TbB_6O_9(OH)_3$ synthesized from a flux of hydroboric acid in Teflon autoclaves [3] are reported in the literature. Interestingly, rare-earth metaborates exhibit various structures depending on the size of the cation, with terbium probably acting as a transition point [9]. For example, the earlier elements *Ln* = La–Nd, Sm–Tb in the lanthanide series $Ln(BO_2)_3$ (*Ln* = La–Nd, Sm–Tb) form the structural α-variant under ambient pressure conditions crystallizing in the monoclinic space group $I2/a$ [5,10–17]. In addition to this monoclinic α-structure, an orthorhombic variant β-$Tb(BO_2)_3$ (space group *Pnma*) was also synthesized depending on the atomic ratio of terbium to boron in the starting materials [6]. The β-variant of the lanthanide metaborate structures was subsequently found for β-$Dy(BO_2)_3$ under ambient [18] and for Nd–Lu at elevated pressures [19–21]. Further high-pressure studies on the metaborates of the early lanthanide elements La–Nd, Sm led to another orthorhombic structure type designated as γ-$Ln(BO_2)_3$ (*Ln* = La–Nd, Sm) [9,22] and even an additional monoclinic variant represented by the compounds δ-$La(BO_2)_3$ and δ-$Ce(BO_2)_3$ [23,24]. The complex polymorphism of the lanthanide orthoborates leads to an even greater structural diversity, which has already been comprehensively outlined in Ref. [25]. These examples impressively demonstrate the structural diversity of lanthanide borates in dependence on synthetic conditions. The abovementioned compounds of the lanthanide meta- and orthoborates were synthesized at relatively high temperatures around 1000 °C and thus, despite the already revealed structural diversity of the lanthanide borates, new discoveries in this field are still to be made through further variation of the experimental parameters. While high temperatures opened the path to substance classes such as for example, borosilicates [26–28], lower temperatures can lead to the formation of hydroxyl- and water-containing compounds as prominently discussed for $LnB_6O_9(OH)_3$ (*Ln* = Sm-Lu) [3], $Ln_4B_6O_{14}(OH)_2$ (*Ln* = Dy, Ho) [29], $DyB_5O_8(OH)_2$ [30], and $Cu_3B_6O_{12} \bullet H_2O$ [31]. Herein, we present a new terbium borate with the composition $Tb_3B_{10}O_{17}(OH)_5$, possessing a new structure type in the realm of

* Corresponding author.
E-mail address: Hubert.Huppertz@uibk.ac.at (H. Huppertz).

https://doi.org/10.1016/j.jssc.2023.124170
Received 3 May 2023; Received in revised form 10 June 2023; Accepted 16 June 2023
Available online 24 June 2023

lanthanide borates synthesized at more moderate temperatures under high-pressure conditions.

2. Experimental section

2.1. High-pressure/high-temperature synthesis of $Tb_3B_{10}O_{17}(OH)_5$

High-pressure/high-temperature syntheses were carried out in a modified Walker-type multianvil press (Max Voggenreither GmbH, Mainleus, Germany), on which a detailed description is found in the related literature [32,33]. For the synthesis of $Tb_3B_{10}O_{17}(OH)_5$, a stoichiometric mixture of Tb_4O_7 (0.08 mmol, Auer-Remy KG, 99.9%) and H_3BO_3 (1.02 mmol, Roth, >99.8%) was filled into a platinum capsule and placed in the center of a 14/8 assembly. Within 267 min, the sample was compressed to 11 GPa, subsequently heated to 700 °C in the following 10 min, and the temperature was kept constant for 30 min. Over the course of the following 78 min, the temperature was incrementally lowered to 200 °C and finally quenched to room temperature. Decompression of the sample was performed within 800 min yielding a colorless product with transparent crystals shown in Fig. 1.

2.2. X-ray crystal structure determination

Transparent single-crystals were isolated under a polarization microscope. Measurements were carried out on a Bruker D8 Quest equipped with a Photon III C14 area detector. The programs SAINT (V8.40B) [34] and APEX4 (v2021.4.0) [35] were used for data collection and processing. A multi-scan absorption correction was carried out using the program SADABS (2016/2) [36,37] and the structure was solved via SHELXT (2018/2) [38,39] algorithms. According to the systematic extinctions h0l with $h + l = 2n$, h00 with $h = 2n$, and 00l with $l = 2n$, candidate space groups were *Pmmn* (no. 59) and $Pmn2_1$ (no. 31). During the crystal structure solution and refinement, the latter space group $Pmn2_1$ (no. 31) was derived since structure solution was successful only under these symmetry conditions. Symmetry checks employing the PLATON program package [40–44] also confirmed the proposed space group $Pmn2_1$. The O–H distances were fixed at 0.83(2) Å using DFIX records and one reflection was omitted from the refinement due to its high deviation. Structure refinements were calculated using SHELXL [45] algorithms incorporated into the program OLEX2 (Version 1.5) [46]. All non-hydrogen atoms were refined anisotropically, and the structure and refinement data are shown in Table 1, Table 2, and Table 3. Selected interatomic distances, bonding angles and hydrogen bonding parameters are provided in Tables 4 and 5 below.

Further details of the crystal structure investigation may be obtained from Fachinformationszentrum Karlsruhe, 76344 Eggenstein-Leopoldshafen, Germany (fax: +49-7247-808-666; e-mail: crysdata@fiz-karlsruhe.de, http://www.fiz-informationsdienste.de/en/DB/icsd/depot_anforderung.html) on quoting the deposition number CSD-2252199.

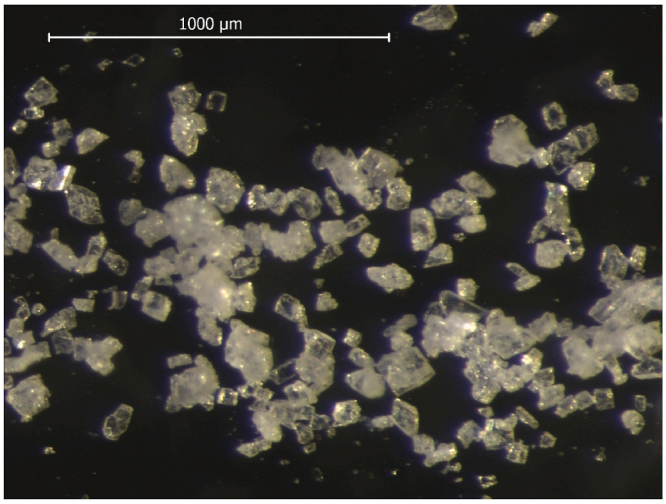

Fig. 1. An optical image of the resulting product.

Table 1
Structural and refinement data for $Tb_3B_{10}O_{17}(OH)_5$.

Empirical formula	$Tb_3B_{10}O_{17}(OH)_5$
Molar mass, g•mol^{-1}	941.90
Crystal system	orthorhombic
Space group	$Pmn2_1$ (no. 31)
Single-crystal data	
a, Å	16.2527(4)
b, Å	4.4373(1)
c, Å	8.8174(2)
Cell volume V, Å^3	635.89(3)
Formula units per cell	2
Calculated density, g•cm^{-3}	4.919
Temperature, K	298(1)
Diffractometer	Bruker D8 Quest Photon III C14
Radiation type; wavelength, pm	Mo-K_α, 71.073
Absorption coefficient, mm^{-1}	16.664
F(000), e	852
Crystal size, mm^3	0.13 × 0.04 × 0.03
Range in θ, deg	2.628–39.440
Range in hkl	$-29 \le h \le 28$ $-7 \le k \le 7$ $-15 \le l \le 15$
Reflections collected	35644
Independent reflections	3859
Reflections with I ≥ 2σ(I)	3850
R_{int}/R_σ	0.0339/0.0215
Completeness to θ = 25.24°, %	98.9
Refinement method	Least squares on F^2
Data/restraints/parameters	3859/4/181
Absorption correction	multi-scan
Flack parameter	0.018(3)
Final R1/wR2 [I ≥ 2σ(I)]	0.0110/0.0254
Final R1/wR2 (all data)	0.0111/0.0254
Goodness-of-Fit on F^2	1.135
Largest diff. peak/hole, e•Å^{-3}	1.352/-2.107
Powder Diffraction Data	
Diffractometer	STOE Stadi P
Radiation; λ, pm	Mo-$K_{\alpha1}$;70.93
a, Å	16.2512(2)
b, Å	4.43745(6)
c, Å	8.8164(2)
Cell volume V, Å^3	634.17(3)
2θ Range, deg	2.000 – 41.960
2θ Step width, deg	0.015
R_{exp}	0.0170
R_{wp}	0.0579
R_p	0.0442

X-ray powder diffraction patterns were collected using a STOE Stadi P Powder Diffractometer (STOE & CIE GmbH, Darmstadt, Germany) [47] equipped with a Ge(111) monochromator and a MYTHEN 1K detector system (Dectris Ltd, Baden-Daettwil, Switzerland) [48]. The measurements were carried out in Debye-Scherrer mode using a 0.7 mm diameter glass capillary (Hilgenberg, Malsfeld, Germany) [49]. The experimental powder diffraction pattern was refined against the crystal structure model obtained from the single-crystal data using the Rietveld-method (Fig. 2) [50,51]. For this purpose, the software TOPAS 4.2 [52] was used.

2.3. Non-linear optical measurements

Second harmonic generation (SHG) measurements were performed on a powder sample of $Tb_3B_{10}O_{17}(OH)_5$ using the Kurtz-Perry approach [53]. We used quartz, KDP (KH_2PO_4), and corundum (Al_2O_3) for reference measurements. A Q-switched Nd:YAG laser (1064 nm, 5–6 ns, 2

Table 2
Atom labels and corresponding Wyckoff-positions, atomic coordinates, and equivalent isotropic displacement parameters (U_{eq}) or isotropic displacement parameter (U_{iso}) for all crystallographically different atoms. U_{eq} is defined as one third of the trace of the U_{ij} tensor (standard deviations in parentheses).

Atom	Wyckoff site	x	y	z	U_{eq}/U_{iso}*
Tb1	4*b*	0.11787(2)	0.42935(2)	0.06904(2)	0.00462(2)
Tb2	2*a*	0	0.44810(3)	0.67610(2)	0.00524(3)
B1	4*b*	0.1519(2)	0.9153(4)	0.8199(2)	0.0045(3)
B2	2*a*	0	0.9256(6)	0.8946(4)	0.0044(4)
B3	2*a*	0	0.9745(7)	0.1967(3)	0.0049(4)
B4	4*b*	0.2768(2)	0.5843(4)	0.2235(3)	0.0046(3)
B5	4*b*	0.1710(2)	0.5715(4)	0.4505(3)	0.0043(3)
B6	4*b*	0.0794(2)	0.0931(5)	0.4259(2)	0.0048(3)
O1	2*a*	0	0.6080(5)	0.9209(2)	0.0048(3)
O2	4*b*	0.15384(9)	0.5834(3)	0.7928(2)	0.0050(2)
O3	4*b*	0.3325(2)	0.0412(3)	0.4873(2)	0.0064(2)
O4	4*b*	0.26359(8)	0.4962(3)	0.0610(2)	0.0047(2)
O5	4*b*	0.19638(9)	0.5251(3)	0.2939(2)	0.0050(2)
O6	4*b*	0.07514(9)	0.0860(3)	0.2631(2)	0.0052(2)
O7	2*a*	0	0.0863(4)	0.0414(2)	0.0049(3)
O8	4*b*	0.09508(9)	0.3995(3)	0.4826(2)	0.0047(2)
O9	4*b*	0.06879(9)	0.0288(4)	0.7996(2)	0.0058(2)
O10	2*a*	0	0.9935(5)	0.4962(2)	0.0045(3)
O11	4*b*	0.20637(9)	0.0847(3)	0.7238(2)	0.0051(2)
O12	2*a*	0	0.6376(5)	0.2062(2)	0.0064(3)
O13	4*b*	0.14899(9)	0.9008(3)	0.4797(2)	0.0049(2)
H3	4*b*	0.286(2)	0.07(2)	0.516(7)	0.03(2)*
H12	2*a*	0	0.58(2)	0.297(4)	0.03(2)*
H13	4*b*	0.165(4)	0.973(9)	0.562(4)	0.04(2)*

kHz) was used for the generation of the fundamental pump wave. The fundamental infrared light was separated using a harmonic separator, a short-pass filter, and an interference filter from the generated second harmonic (532 nm). The generated SHG signal was collected with a photomultiplier and an oscilloscope from 6 different areas of the sample. On each position, 64 pulses were measured and averaged. Background signals between the laser pulses were used to correct the measured intensities. The SHG measurements were performed under ambient conditions in transmission geometry.

2.4. Infrared spectroscopy

Infrared spectra of the new compound were collected on a Bruker Alpha Platinum attenuated total reflection (ATR) spectrometer on the bulk material. The spectra were measured in the range of 4000 to 400 cm^{-1} and the data were processed and corrected for atmospheric influences employing the OPUS 7.2 [54] software.

2.5. Energy-dispersive X-ray spectroscopy (EDX)

A polycrystalline sample of $Tb_3B_{10}O_{17}(OH)_5$ was analyzed via EDX, using a Zeiss EVO® MA10 scanning electron microscope in the variable pressure (60 Pa of N_2) mode. The microscope was equipped with an LaB_6 cathode and an EDX detector from Oxford Instruments. A backscattered electron detector (BSD) was used for imaging with an acceleration voltage of 20 keV. TbF_3, Pt, and SiO_2 were used as standards for terbium, platinum, and oxygen.

2.6. Temperature-dependent X-ray powder diffraction

The thermal behavior of $Tb_3B_{10}O_{17}(OH)_5$ was examined by high-temperature powder X-ray diffraction. For the measurements, the sample was filled into a quartz glass capillary (0.3 mm outer diameter, Hilgenberg, Malsfeld) and heated from 40 to 1000 °C in steps of 20 °C with a heating rate of 10 °C/min. After each temperature step during heating, powder X-ray diffraction data were collected within 90 min at a constant temperature. After this procedure, the heating was switched off and another measurement was carried out at room temperature. Data collection was performed on a STOE Stadi P diffractometer (STOE & Cie GmbH, Darmstadt), using Ge(111) monochromatized Ag-$K\alpha_1$ radiation (λ = 0.5594217 Å) and an IP-PSD detector equipped with a STOE resistance graphite furnace for temperature control.

3. Results and discussion

3.1. Crystal structure of $Tb_3B_{10}O_{17}(OH)_5$

The orthorhombic structure of $Tb_3B_{10}O_{17}(OH)_5$ shows unit cell parameters of a = 16.2527(4), b = 4.4373(1), c = 8.8174(2) Å, and a volume of 635.9(1) $Å^3$. It crystallizes non-centrosymmetrically in the space group $Pmn2_1$ (no. 31) with two formula units per unit cell (single-crystal data).

The two crystallographically different terbium-centered polyhedra are shown in Fig. 3. Interatomic distances vary from 2.351(2) to 3.073 (2) Å for the ten-fold coordinated Tb1 and from 2.273(3) to 3.012(2) Å for the eleven-fold coordinated Tb2 site, which is comparable with Tb–O-bonds in other known terbium borates [4–8,55]. However, it is apparent that the interatomic distances around the Tb2 site are larger than those around the Tb1 atom. Likely, this is the result of the higher

Table 3
Anisotropic displacement parameters for all crystallographic different non-hydrogen atoms.

Atom	U_{11}	U_{22}	U_{33}	U_{23}	U_{13}	U_{12}
Tb1	0.00397(3)	0.00446(3)	0.00542(3)	0.00033(3)	0.00012(3)	−0.00009(2)
Tb2	0.00554(4)	0.00656(4)	0.00360(5)	−0.00064(4)	0	0
B1	0.0041(7)	0.0045(7)	0.0050(7)	0.0004(5)	−0.0004(6)	0.0002(5)
B2	0.0033(9)	0.0056(11)	0.004(2)	−0.0001(7)	0	0
B3	0.0039(9)	0.0050(9)	0.006(2)	−0.0014(8)	0	0
B4	0.0053(7)	0.0044(7)	0.0039(7)	−0.0002(5)	−0.0007(6)	0.0000(5)
B5	0.0043(6)	0.0046(7)	0.0041(7)	0.0000(5)	0.0003(6)	−0.0008(5)
B6	0.0047(7)	0.0048(7)	0.0048(7)	−0.0002(5)	−0.0002(6)	0.0001(5)
O1	0.0066(7)	0.0027(6)	0.0049(7)	0.0003(5)	0	0
O2	0.0049(5)	0.0039(5)	0.0061(5)	−0.0007(4)	0.0020(5)	0.0002(4)
O3	0.0064(5)	0.0070(5)	0.0058(5)	−0.0011(4)	−0.0018(4)	0.0012(4)
O4	0.0044(4)	0.0050(4)	0.0046(5)	−0.0014(4)	0.0003(4)	0.0003(4)
O5	0.0039(5)	0.0073(5)	0.0038(5)	−0.0007(4)	0.0005(4)	−0.0007(4)
O6	0.0050(5)	0.0069(5)	0.0038(5)	−0.0001(4)	−0.0011(4)	−0.0010(4)
O7	0.0066(7)	0.0043(7)	0.0038(7)	0.0003(5)	0	0
O8	0.0045(4)	0.0037(5)	0.0059(5)	−0.0011(4)	0.0006(4)	−0.0010(4)
O9	0.0038(5)	0.0071(5)	0.0063(6)	0.0026(4)	0.0009(4)	0.0012(4)
O10	0.0028(6)	0.0056(7)	0.0052(7)	0.0012(6)	0	0
O11	0.0051(5)	0.0046(5)	0.0057(5)	−0.0001(4)	0.0015(4)	−0.0008(4)
O12	0.0102(8)	0.0042(7)	0.0047(7)	0.0003(6)	0	0
O13	0.0051(4)	0.0041(5)	0.0055(5)	−0.0009(4)	−0.0017(4)	0.0015(4)

Table 4
Selected interatomic distances (Å) and bond angles (deg) (standard deviations in parentheses).

Atoms	Distance	Atoms	Distance	Atoms	Distance
Tb1–O3[a]	2.351(2)			Tb2–O1	2.273(3)
Tb1–O4	2.388(2)			Tb2–O8[e]	2.312(2)
Tb1–O6	2.394(2)			Tb2–O8	2.312(2)
Tb1–O5	2.396(2)			Tb2–O9[e]	2.428(2)
Tb1–O12	2.447(2)			Tb2–O9	2.428(2)
Tb1–O1[b]	2.450(2)			Tb2–O10[d]	2.566(3)
Tb1–O7	2.459(2)			Tb2–O2[e]	2.770(2)
Tb1–O3[c]	2.586(2)			Tb2–O2	2.770(2)
Tb1–O2[b]	2.597(2)			Tb2–O10	2.893(3)
Tb1–O9[d]	3.073(2)			Tb2–O9[f]	3.012(2)
				Tb2–O9	3.012(2)
average	2.514			average	2.616
B1–O11[f]	1.438(3)	B2–O1	1.428(4)	B3–O6[f]	1.442(3)
B1–O9[f]	1.452(3)	B2–O9[h]	1.470(3)	B3–O6[h]	1.442(3)
B1–O2	1.492(3)	B2–O9[f]	1.402(3)	B3–O7[f]	1.457(4)
B1–O3[g]	1.510(3)	B2–O7[i]	1.478(4)	B3–O12	1.498(4)
average	1.473	average	1.4445	average	1.45975
B4–O5	1.470(3)	B5–O5	1.456(3)	B6–O6	1.437(3)
B4–O2[c]	1.483(3)	B5–O4[g]	1.473(3)	B6–O8	1.471(3)
B4–O11[c]	1.494(3)	B5–O8	1.478(3)	B6–O13[d]	1.494(3)
B4–O4	1.501(3)	B5–O13	1.526(3)	B6–O10[d]	1.499(3)
average	1.487	average	1.48325	average	1.47525

Atoms	Angle	Atoms	Angle	Atoms	Angle
O9[f]–B1–O3[g]	103.4 (2)	O9[h]–B2–O9[f]	99.0 (3)	O6[f]–B3–O7[f]	105.4 (2)
O11[f]–B1–O9[f]	108.6 (2)	O1–B2–O7[i]	109.5 (3)	O6[h]–B3–O7[f]	105.4 (2)
O2–B1–O3[g]	106.2 (2)	O9[h]–B2–O7[i]	110.4 (2)	O6[f]–B3–O12	108.7 (2)
O9[f]–B1–O2	110.0 (2)	O9[f]–B2–O7[i]	110.4 (2)	O6[h]–B3–O12	108.7 (2)
O11[f]–B1–O2	114.1 (2)	O1–B2–O9[h]	113.6 (2)	O7[f]–B3–O12	113.1 (3)
O11[f]–B1–O3[g]	114.0 (2)	O1–B2–O9[f]	113.6 (2)	O6[f]–B3–O6[h]	115.8 (3)
average	109.4	average	109.4	average	109.5
O5–B4–O4	103.3 (2)	O4[g]–B5–O13	104.7 (2)	O8–B6–O10[d]	106.3 (2)
O11[c]–B4–O4	106.5 (2)	O8–B5–O13	105.5 (2)	O8–B6–O13[d]	106.8 (2)
O5–B4–O11[c]	109.8 (2)	O5–B5–O8	110.2 (2)	O6–B6–O13[d]	110.0 (2)
O2[c]–B4–O11[c]	110.7 (2)	O5–B5–O13	111.2 (2)	O13[d]–B6–O10[d]	110.6 (2)
O2[c]–B4–O4	111.8 (2)	O4[g]–B5–O8	111.8 (2)	O6–B6–O10[d]	111.4 (2)
O5–B4–O2[c]	114.4 (2)	O5–B5–O4[g]	113.2 (2)	O6–B6–O8	111.6 (2)
average	109.4	average	109.4	average	109.5

Symmetry operators for generating equivalent atoms.
[a] -x+0.5, -y, z-0.5.
[b] x, y, z-1.
[c] -x+0.5, -y+1, z-0.5.
[d] x, y-1, z.
[e] -x, y, z.
[f] x, y+1, z.
[g] -x+0.5, -y+1, z+0.5.
[h] -x, y+1, z.
[i] x, y+1, z+1.

coordination number [56]. The terbium atoms are arranged in triple-chains running along the crystallographic *b*-axis, where two face-sharing [$Tb1O_{10}$] polyhedra are linked, again *via* face-sharing, to one [$Tb2O_{11}$] polyhedron.

Within the six crystallographically different [BO_4] tetrahedra, the interatomic B–O distances display an average value of 1.472 Å. This is close to the value of 1.476(35) Å, which is often referred to as the standard bond length in tetrahedral [BO_4] units [57]. The average

Table 5
Hydrogen bond parameters in $Tb_3B_{10}O_{17}(OH)_5$.

Atoms	D–H/Å	H•••A/Å	D–H•••A/Å	D–H•••A/deg
O3–H3•••O4	0.80(3)	2.13(5)	2.660(3)	123.7
O3–H3•••O11	0.80(3)	2.25(6)	2.931(3)	143.5
O3–H3•••O13	0.80(3)	2.37(4)	3.048(3)	142.1
O12–H12•••O8	0.83(3)	2.39(4)	3.073(3)	138.8
O13–H13•••O11	0.83(3)	1.65(5)	2.483(3)	172.7

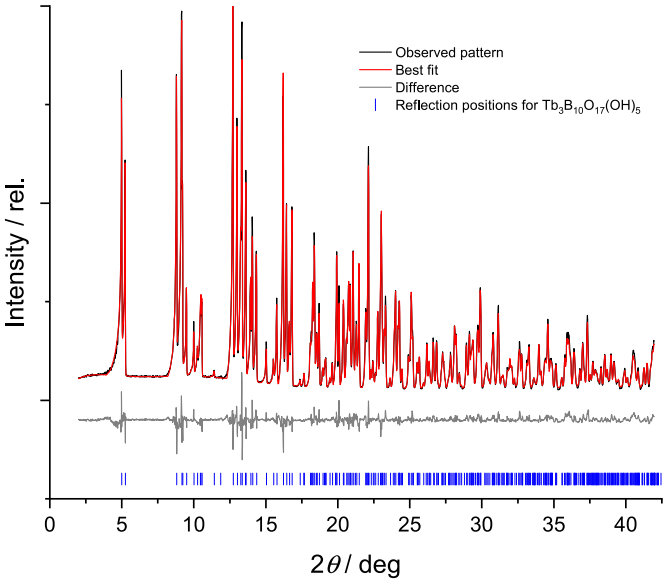

Fig. 2. Powder X-ray diffraction pattern and Rietveld-refinement of $Tb_3B_{10}O_{17}(OH)_5$ (λ = 70.93 pm).

bonding angles within the [BO_4] tetrahedra being 109.4° for the B1, B2, B4, and B5 and 109.5° for the B3 and B6 tetrahedra correlate well with the expected regular tetrahedral angle of 109.4°. Since only a slight variation of the individual bonding angles around this value is observed, the tetrahedra can be described as nearly undistorted. *Via* corner-sharing, the [BO_4] tetrahedra form a three-dimensional framework that can be described by corrugated layers in the *ab*-plane, which are further linked along the crystallographic *c*-axis. The corrugated layers, which are shown in Fig. 4, are built up of planar six-membered rings, distorted six-membered rings, and corrugated eight-membered rings.

The connection of two adjacent layers is highlighted in the following Fig. 5. The B3 tetrahedra are linked *via* the O6 atoms to two B6 tetrahedra of one layer and *via* the O7 to one B2 tetrahedron of an adjacent layer. Furthermore, two adjacent layers are linked via the O4 atoms through corner-sharing of the B4 and B5 tetrahedra.

For a graphical depiction of the resulting crystal structure of the new compound, the reader is referred to Fig. 6. Thus, it is also apparent that two adjacent layers are offset ½ in crystal coordinates along the *a*-axis leading to an ABABA-stacking of the described corrugated layers.

During the refinement, the position of the protons could be determined based on the coordination geometry around the boron and oxygen atoms and therefore, we included them in Figs. 3–5. As a result of the formation of a hydroxyl-group, we expect the respective B–O-distance to be elongated and hence, also the [BO_4] tetrahedron would be more distorted, which should be apparent from the O–B–O-angles within the coordination sphere of a respective boron atom. Furthermore, it is safe to assume that the hydrogen atoms will occupy sites, which are sterically not too hindered by the coordination spheres of the terbium or other boron atoms. Thus, four oxygen sites were identified on which the hydrogen atoms could be located: the O3, O11, O12, and O13 atom,

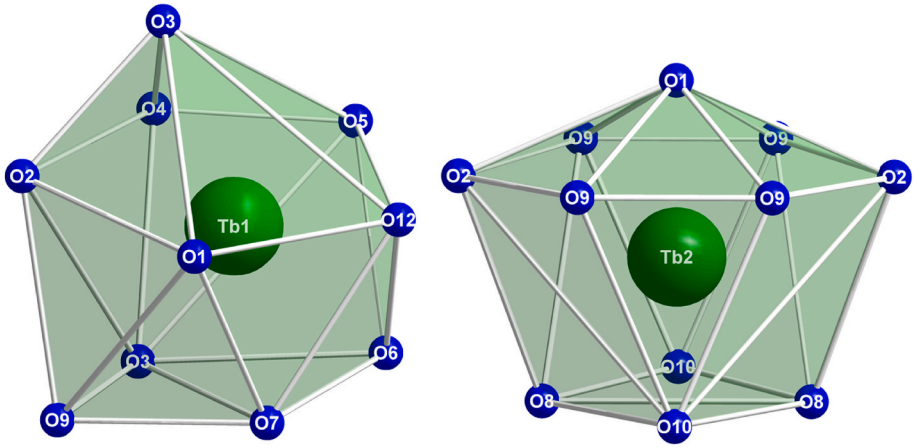

Fig. 3. The coordination spheres of the two crystallographic different terbium-centered polyhedra.

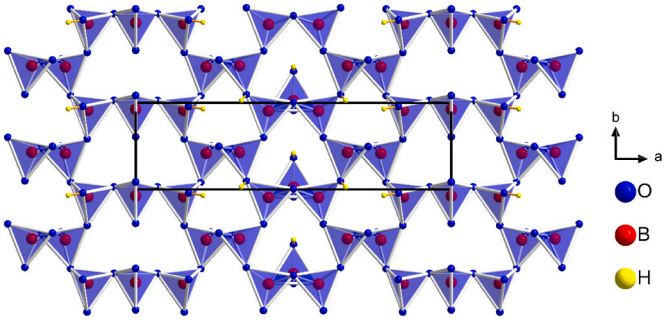

Fig. 4. View of the layers of six- and eight-membered rings, which are then further connected to yield the three-dimensional borate-framework.

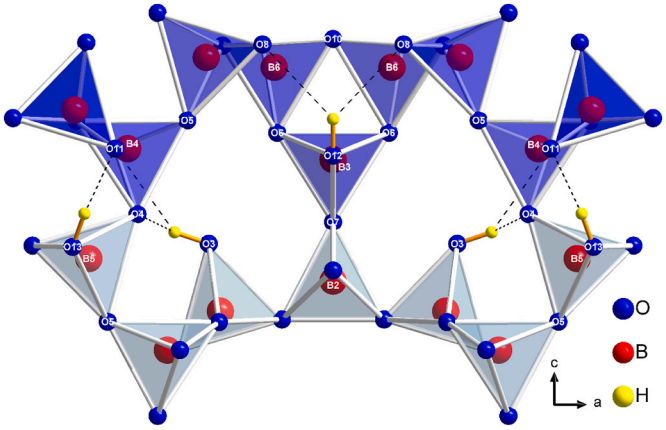

Fig. 5. The connection of two adjacent layers and the hydrogen positions are highlighted.

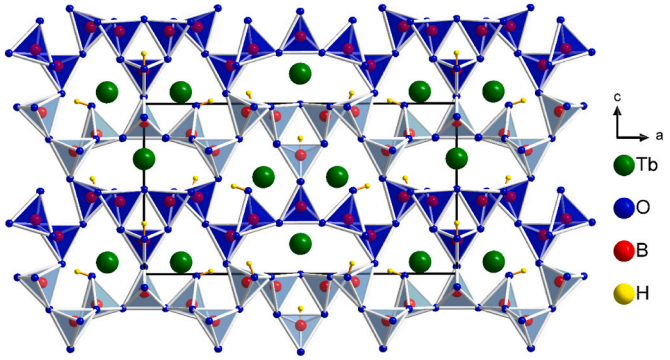

Fig. 6. View on the expanded unit cell of $Tb_3B_{10}O_{17}(OH)_5$. Layers of six- and eight-membered rings in the *ab*-plane are connected along the *c*-axis to yield a three-dimensional framework where two adjacent layers are offset ½ in crystal coordinated along the *a*-axis.

which is apparent from the coordination spheres of all crystallographically different oxygen atoms shown in Fig. 7. With reasonable displacement parameters, the hydrogen atoms could only be refined to the O3, O12, and O13 atoms, yielding five protons in total, which is the exact amount needed for charge neutrality, assuming the oxidation state + III for the terbium atoms.

To further investigate our working hypotheses, we calculated the bond valences of all crystallographically different non-hydrogen atoms according to the bond-length/bond-strength [58] (BLBS) and charge distribution [59] (CHARDI) concept (Table 6). Hydrogen bonds with hydrogen-donor-distances up to 2.4 Å (listed in Table 5) were considered to contribute significantly to the bond valences of a given atom in the BLBS-calculations. These results indeed indicate the oxidation state + III for the two crystallographically different terbium atoms and the bond valences of the oxygen atoms are in good congruency with the expected value of −2. Therefore, we assume that also the previously proposed positions of the hydrogen atoms at the O3, O12, and the O13 atoms are correct.

After the assignment of the positions of the hydrogen atoms, a more detailed look into H-bonding of the new compound concludes the description of its crystal structure. In Fig. 5, a graphical depiction of the chemical environment of the hydrogen atoms in the structure is also shown. Generally, linear contacts with D−H•••A-angles higher than 120° are favored for the formation of H-bonds. Interatomic D−H•••A-distances up to 3.2 Å can then be considered as possible H-bonds [60], but in the following, we will focus on the stronger H-bonds with D−H•••A distances around 3 Å. Judging from the geometric parameters, the H-bond between the atoms O13–H13•••O11 should be the strongest since it is not only the most linear, but also displays an interatomic H13•••O11-distance of 1.65(5) Å, which is significantly shorter than the other distances between hydrogen and possible acceptor atoms in $Tb_3B_{10}O_{17}(OH)_5$. At a D−H•••A-distance of 2.931(3) Å, the O11 also acts as an acceptor for the H3 atom forming one of the three H-bonds of this hydrogen. The other two acceptor oxygen atoms, O4 and O13, are found at D−H•••A-distances of 2.660(3) Å and 3.048(3) Å, respectively. For the H12, only the O8 is found as a possible H-acceptor within reasonable geometric parameters with a D−H•••A-distance of 3.073 Å and an angle of 138.8°.

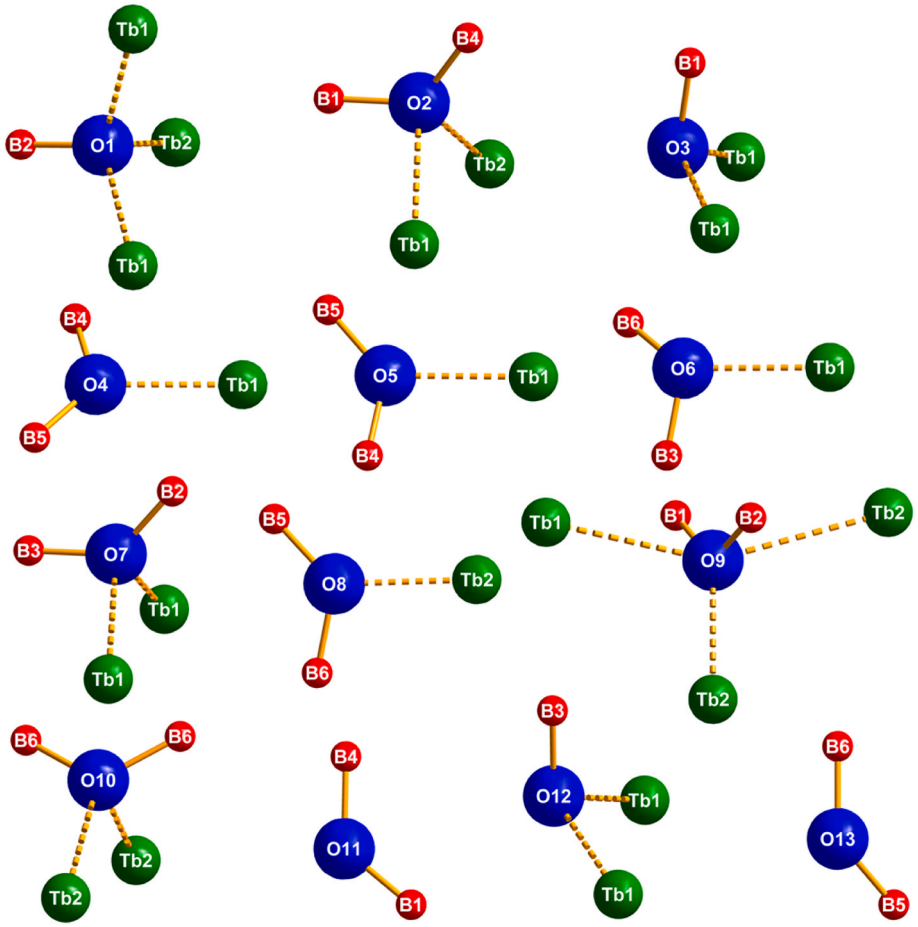

Fig. 7. The coordination spheres of all 13 crystallographically different oxygen atoms. It is apparent from the coordination environments of all oxygen atoms that only four atoms namely O3, O11, O12, and O13, are reasonable candidates to bind to a hydrogen atom, which are not shown here.

Table 6
Calculation of bond valences with BLBS [58] (∑V) and CHARDI-2015 [59] (∑Q).

Atom	Without hydrogen		Hydrogen at O3, O12, and O13	
	∑V	∑Q	∑V	∑Q
Tb1	3.02	3.55	3.02	2.91
Tb2	2.89	3.05	2.89	3.04
B1	3.04	3.68	3.04	3.17
B2	3.13	2.95	3.13	2.98
B3	3.15	3.26	3.15	2.89
B4	2.92	3.33	2.92	3.14
B5	2.96	3.35	2.96	2.97
B6	3.02	3.45	3.02	3.04
O1	−2.02	−2.08	−2.02	−2.02
O2	−1.81	−1.78	−1.81	−1.92
O3	−1.33	−1.28	−2.30	−2.03
O4	−1.85	−1.87	−1.99	−1.99
O5	−1.93	−2.01	−1.93	−1.98
O6	−2.03	−2.05	−2.04	−2.03
O7	−2.17	−2.11	−2.17	−2.05
O8	−1.98	−2.05	−2.05	−1.99
O9	−1.91	−1.95	−1.91	−1.96
O10	−1.75	−1.68	−1.75	−1.97
O11	−1.55	−1.59	−2.17	−1.93
O12	−1.36	−1.30	−2.25	−2.17
O13	−1.43	−1.31	−2.33	−2.06

3.2. Non-linear optical properties of $Tb_3B_{10}O_{17}(OH)_5$

In Table 7, the measured SHG-intensities of all investigated samples are provided. SHG-measurements on a powder sample of $Tb_3B_{10}O_{17}(OH)_5$ yielded an intensity of 141(32) mV, which is about 39% of the respective SHG-signal of quartz. Thus, the non-centrosymmetric space group $Pmn2_1$ of the new terbium borate is confirmed [53]. The point group *mm*2 has five independent SHG coefficients, namely, d_{31}, d_{15}, d_{32}, d_{24}, and d_{33} [61]. If the Kleinman symmetry relations [62] are valid, $d_{31} = d_{15}$ and $d_{24} = d_{32}$, because all three subscripts of the SHG tensor can be permutated by neglecting dispersion. However, the Kurtz-Perry approach [53] usually provides information about the averaged effective SHG coefficient with large uncertainty and helps in estimating the order of magnitude of SHG coefficients. The low SHG intensity indicates a non-phase-matching condition.

Table 7
Comparison of SHG-intensities of $Tb_3B_{10}O_{17}(OH)_5$ with known centrosymmetric and non-centrosymmetric reference samples.

Samples	SHG intensities [mV]	I_{SHG}/I_{Quartz}•100%
Quartz (<5 μm)	24(5)	7
Quartz (5–25 μm)	178(50)	50
Quartz (25–50 μm)	358(88)	100
Al_2O_3 (9 μm)	0 (1)	0
KDP (5–25 μm)	744(160)	208
KDP (25–50 μm)	3148(960)	879
$Tb_3B_{10}O_{17}(OH)_5$ (30–70 μm)	141(32)	39

3.3. Infrared spectroscopy

In the ATR-IR spectrum of the new compound (Fig. 8), the signal at 3432 cm^{-1} stems from the OH-stretching modes, which are expected in

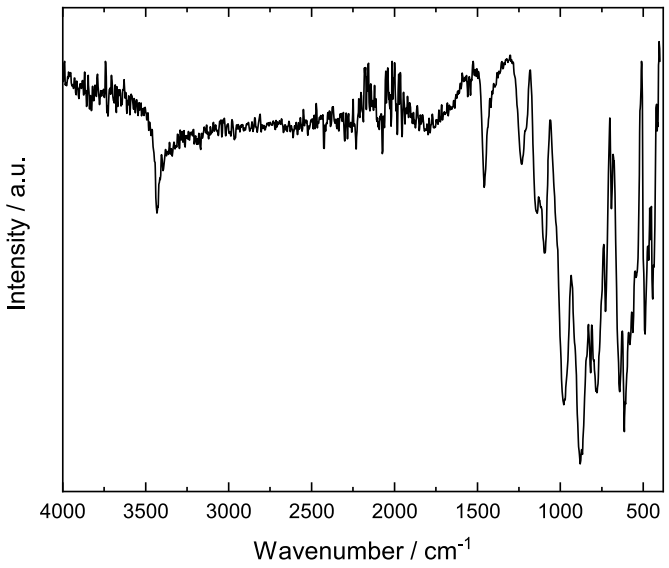

Fig. 8. The ATR-infrared spectrum of the bulk-material $Tb_3B_{10}O_{17}(OH)_5$.

$Tb_3B_{10}O_{17}(OH)_5$ [63]. Stretching modes of the [BO_4] tetrahedra are generally expected in the range from 1100 to 850 cm^{-1} [64]. Outside this range, three additional signals at wavenumbers 1148, 1232, and 1458 cm^{-1} are observed. Due to the absence of trigonal [BO_3] groups in the structure, these signals probably come from contributions of B–O–B, O–B–O, and Tb–O–B vibrations. Similar signals were reported for β-ZnB_4O_7 and β-CaB_4O_7, where ab-initio quantum chemical calculations confirmed the experimental results [65]. Bending modes of the borate framework are visible in the lower wavenumber range of the presented infrared spectrum (Fig. 8) [64].

3.4. Energy-dispersive X-ray spectroscopy

Fig. 9 shows a picture of the sample in which the locations of the single-spot measurements are marked. The presence of oxygen was confirmed but cannot be quantitatively determined with significant certainty via EDX. A mapping of a larger area (4.18 × 3.13 mm^2) of crystals revealed a uniform distribution around the average values of 12 (3) % terbium and 88(3) % oxygen. Three small areas (each approximately 800 μm^2) show residuals of platinum, probably from the platinum capsule used during the synthesis. The quantification of hydrogen and boron is not accessible via EDX. The mapping as well as single point measurements showed no sign of further impurities.

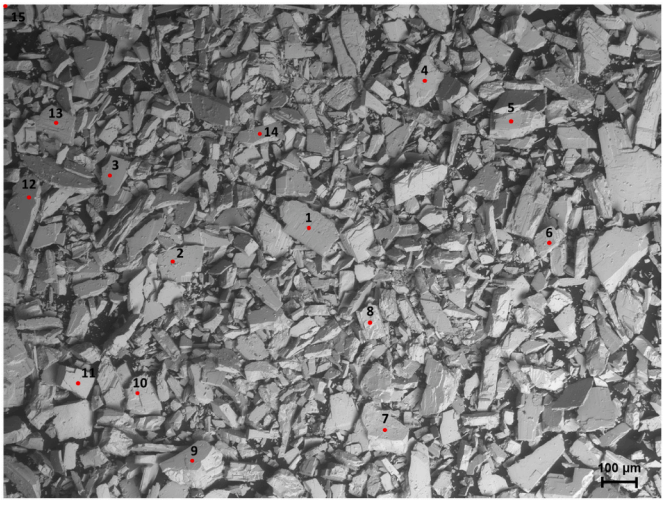

Fig. 9. A polycrystalline sample was investigated using EDX. Single-spot measurements are marked with numbers from 1 to 15.

3.5. Thermal stability and behavior

On the compounds $Dy_4B_6O_{15}$ [66] and $Dy_4B_6O_{14}(OH)_2$ [29], it was previously discussed that the protonated species plays the role of an intermediate product in the synthesis of the hydrogen-free compound as water is eliminated from the structure upon a rise in temperature [29]. Thus, judging from the experimental parameters used for the synthesis of $Tb_3B_{10}O_{17}(OH)_5$, the formation of a protonated species was expected. Using high-temperature X-ray powder diffractometry at ambient pressure, the thermal stability of $Tb_3B_{10}O_{17}(OH)_5$ was studied in detail. In the 2θ-range from 3 to 30°, the temperature-dependent X-ray powder diffraction data are shown in Fig. 10.

As apparent from Fig. 11, no significant changes in the powder diffraction patterns are found up to 460 °C, aside from a small shift of the reflection positions.

Reflections assigned to the crystal structure of $Tb_3B_{10}O_{17}(OH)_5$ remain present up to 680 °C, while the formation of β-$Tb(BO_2)_3$ [6] (Fig. 12) is observed. The broad temperature range of this phase transition is likely explained by time dependency of the reaction.

At temperatures above 920 °C, the sample consists of μ-$TbBO_3$ [67] (Fig. 13), which is then stable up to at least 1000 °C and transforms to π-$TbBO_3$ [68] upon cooling to room temperature (Fig. 14). These findings are coherent with previous works on the thermal behavior of lanthanide meta- and orthoborates of Becker and Fröhlich [7] and Lin et al. [67].

For an estimation of thermal expansion factors, the unit cell parameters of $Tb_3B_{10}O_{17}(OH)_5$ were determined in the temperature range from 40 to 460 °C *via* Rietveld-refinements of the temperature-dependent X-ray powder patterns. In Fig. 15, the change of the unit cell parameters as a function of the temperature is depicted.

4. Conclusion

In this work, we present the high-pressure/high-temperature synthesis of the new non-centrosymmetric terbium borate $Tb_3B_{10}O_{17}(OH)_5$ at 11 GPa and 650 °C followed by the determination of its crystal structure by single-crystal X-ray diffraction methods. $Tb_3B_{10}O_{17}(OH)_5$ exhibits a three-dimensional framework built up of corner-sharing

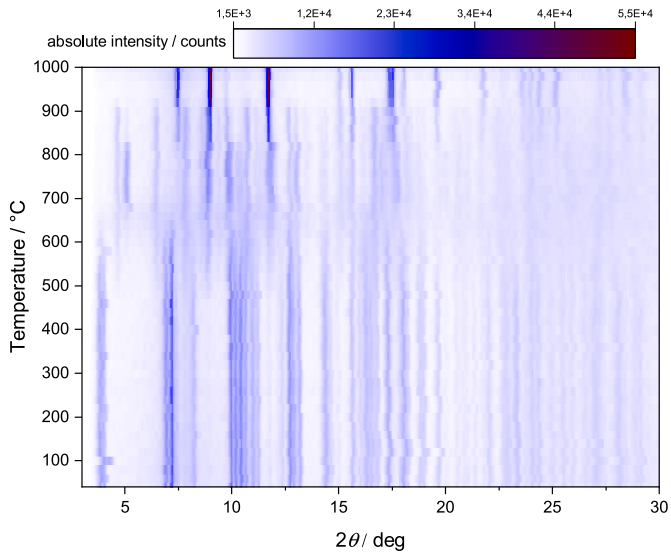

Fig. 10. Heatmap-diagram of the temperature-dependent X-ray powder diffraction measurements (λ = 55.94 pm) on the new compound $Tb_3B_{10}O_{17}(OH)_5$ in the range from 3 to 30°.

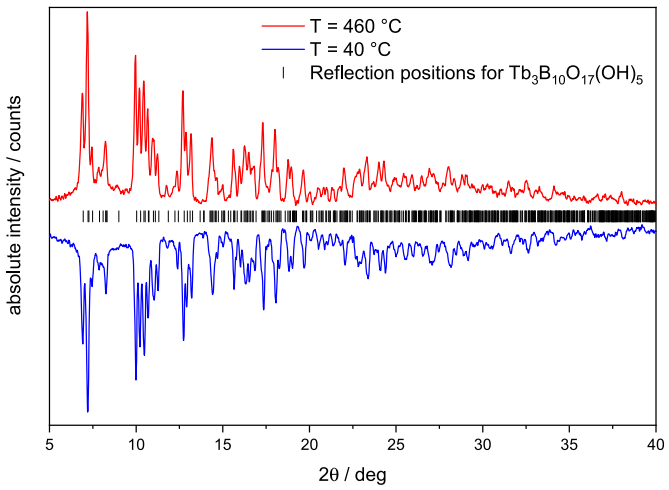

Fig. 11. Apart from a small shift of the reflection positions, no significant changes in the powder pattern ($\lambda = 55.94$ pm) of $Tb_3B_{10}O_{17}(OH)_5$ are observed in the range from 40 to 460 °C. Therefore, we conclude that the compound is stable in this temperature range.

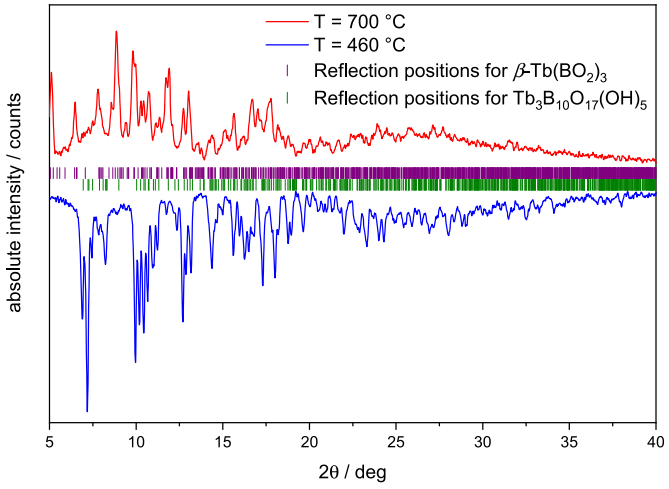

Fig. 12. Between 460 and 700 °C, a time-dependent reaction yielding β-$Tb(BO_2)_3$ [6] is observed by the change of the powder pattern ($\lambda = 55.94$ pm).

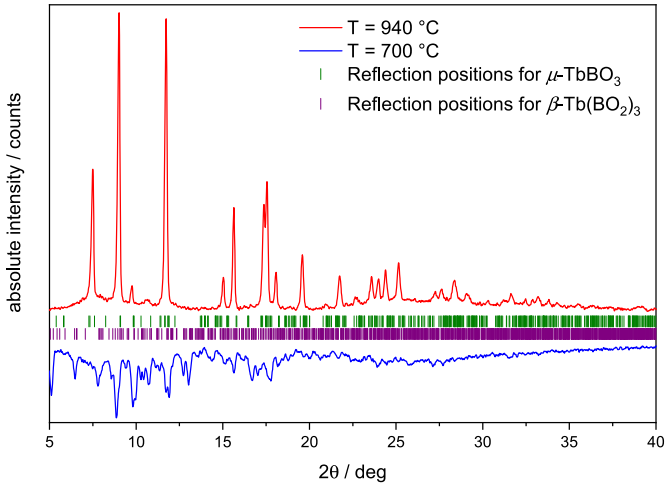

Fig. 13. β-$Tb(BO_2)_3$ [6] is transformed to μ-$TbBO_3$ [67] after heating to 940 °C ($\lambda = 55.94$ pm).

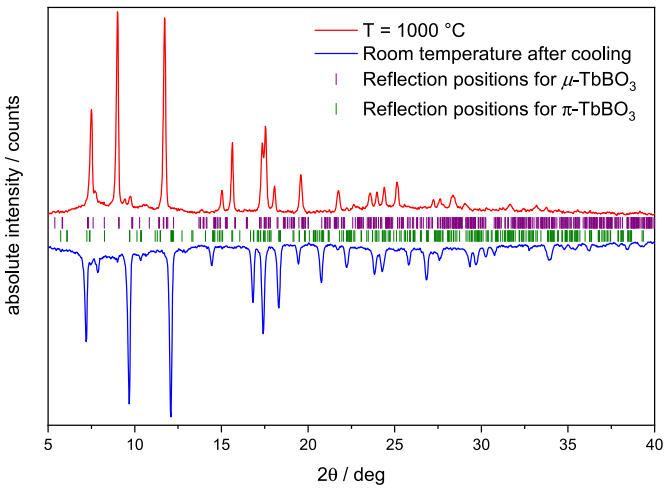

Fig. 14. μ-$TbBO_3$ [67] transforms to π-$TbBO_3$ [68] upon cooling to room temperature ($\lambda = 55.94$ pm).

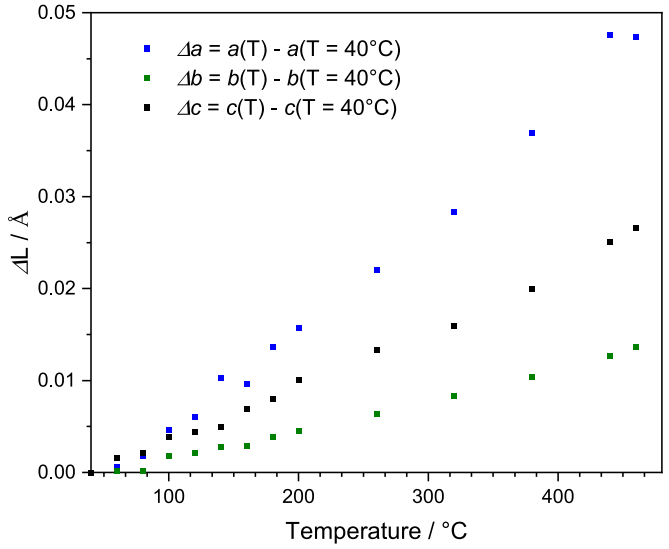

Fig. 15. Change of unit cell parameters of $Tb_3B_{10}O_{17}(OH)_5$, obtained *via* Rietveld-refinements, as a function of the temperature. The unit cell parameters at 40 °C $a = 16.292(2)$ Å, $b = 4.4485(3)$ Å, and $c = 8.8369(7)$ Å were used as a zero-point.

$[BO_4]$ tetrahedra. The single-crystal X-ray data are accompanied by Rietveld-refinements of the experimental powder diffraction patterns, an infrared-spectroscopic investigation, SHG measurements, temperature-dependent X-ray powder diffraction, and an EDX-analysis of the chemical composition of the X-ray pure sample. At temperatures higher than 460 °C, β-$Tb(BO_2)_3$ forms from $Tb_3B_{10}O_{17}(OH)_5$ in a time-dependent reaction. A further raise in temperature to 940 °C leads to the formation of μ-$TbBO_3$, which transforms into π-$TbBO_3$ upon cooling.

CRediT authorship contribution statement

Tobias A. Teichtmeister: Writing – original draft, Investigation, Visualization, Data curation. **Christian Paulsen:** Investigation, Writing – review & editing. **Sebastian J. Ambach:** Investigation, Writing – review & editing. **Klaus Wurst:** Validation. **Lkhamsuren Bayarjargal:** Investigation, Resources, Writing – review & editing. **Wolfgang Schnick:** Writing – review & editing, Resources. **Hubert Huppertz:** Writing – review & editing, Resources.

Declaration of competing interest

The authors declare that they have no known competing financial interests or personal relationships that could have appeared to influence the work reported in this paper.

Data availability

The crystal structure investigation http://www.fiz-informationsdienste.de/en/DB/icsd/dep Deposition number CSD-2252199.

Acknowledgement

The authors want to thank the Vice Rector for Research for the grant of a doctoral fellowship at the University of Innsbruck.

Appendix A. Supplementary data

Supplementary data to this article can be found online at https://doi.org/10.1016/j.jssc.2023.124170.

References

[1] M. Mutailipu, K.R. Poeppelmeier, S. Pan, Borates: a rich source for optical materials, Chem. Rev. 121 (2021) 1130–1202, https://doi.org/10.1021/acs.chemrev.0c00796.
[2] H. Huppertz, R. Ziegler, 6.3 Borate applications, in: R. Pöttgen, T. Jüstel, C. A. Strassert (Eds.), From Energy Storage to Photofunctional Materials, De Gruyter, 2022, pp. 153–165.
[3] L. Li, P. Lu, Y. Wang, X. Jin, G. Li, Y. Wang, L. You, J. Lin, Synthesis of rare earth polyborates using molten boric acid as a flux, Chem. Mater. 14 (2002) 4963–4968, https://doi.org/10.1021/cm0203870.
[4] P. Mukherjee, E. Suard, S.E. Dutton, Magnetic properties of monoclinic lanthanide metaborates, $Ln(BO_2)_3$, Ln = Pr, Nd, Gd, Tb, J. Phys. Condens. Matter 29 (2017), 405807, https://doi.org/10.1088/1361-648X/aa8160.
[5] A. Goriounova, P. Held, P. Becker, L. Bohatý, Monoclinic modification of polymorphic TbB_3O_6, Acta Crystallogr. E59 (2003) i83–i85, https://doi.org/10.1107/S1600536803009553.
[6] T. Nikelski, T. Schleid, Synthese und Kristallstruktur von Terbium(III)-*meta*-Oxoborat $Tb(BO_2)_3$ (≡ TbB_3O_6), Z. Anorg. Allg. Chem. 629 (2003) 1017–1022, https://doi.org/10.1002/zaac.200200446.
[7] P. Becker, R. Fröhlich, Polymorphy of monoclinic terbium triborate, TbB_3O_6, Cryst. Res. Technol. 43 (2008) 1240–1246, https://doi.org/10.1002/crat.200800397.
[8] H. Emme, H. Huppertz, High-pressure preparation, crystal structure, and properties of α-$(RE)_2B_4O_9$ (RE = Eu, Gd, Tb, Dy): oxoborates displaying a new type of structure with edge-sharing BO_4 tetrahedra, Chem. Eur J. 9 (2003) 3623–3633, https://doi.org/10.1002/chem.200204696.
[9] H. Emme, C. Despotopoulou, H. Huppertz, High-pressure synthesis and crystal structure of the structurally new orthorhombic rare-earth *meta*-oxoborates γ-$RE(BO_2)_3$ (RE = La-Nd), Z. Anorg. Allg. Chem. 630 (2004) 2450–2457, https://doi.org/10.1002/zaac.200400202.
[10] G.K. Abdullaev, K. Mamedov, G.G. Dzhafarov, Crystal Structures of the Metaborates $Sm(BO_2)_3$ and $Gd(BO_2)_3$, Kristallografiya, 1975, pp. 265–269.
[11] G.K. Abdullaev, K. Mamedov, G.G. Dzhafarov, The refined crystal structure of lanthanum metaborate $La(BO_2)_3$, Kristallografiya (1981) 837–840.
[12] A. Goriounova, P. Held, P. Becker, L. Bohatý, Cerium triborate, CeB_3O_6, Acta Crystallogr. E60 (2004) i134–i135, https://doi.org/10.1107/S1600536804024365.
[13] A. Goriounova, P. Held, P. Becker, L. Bohatý, Europium triborate, EuB_3O_6, Acta Crystallogr. E60 (2004) i131–i133, https://doi.org/10.1107/S1600536804024353.
[14] H. Müller-Bunz, T. Nikelski, T. Schleid, Einkristalle des Neodym(III)-*meta*-Borats $Nd(BO_2)_3$ und -*ortho*-Borats $Nd[BO_3]$, Z. Naturforsch. 58b (2003) 375–380, https://doi.org/10.1515/znb-2003-0503.
[15] V.I. Pakhomov, G.B. Silnitskaya, A.V. Medvedev, B.F. Dzhurinskii, The crystal structure of neodymium metaborate, Izv. Akad. Nauk. SSSR - Neorganicheskiye Mater. (1972) 1259–1263.
[16] C. Sieke, T. Nikelski, T. Schleid, $Pr(BO_2)_3$ und $PrCl(BO_2)_2$: zwei meta-Borate des Praseodyms im Vergleich, Z. Anorg. Allg. Chem. 628 (2002) 819, https://doi.org/10.1002/1521-3749(200205)628:4<819:AID-ZAAC819>3.0.CO;2-E.
[17] J. St Ysker, W. Hoffmann, Die Kristallstruktur des $La[B_3O_6]$, Naturwissenschaften 57 (1970) 129, https://doi.org/10.1007/BF00600055.
[18] T. Nikelski, M.C. Schäfer, H. Huppertz, T. Schleid, Crystal structure of dysprosium meta-oxoborate, β-$Dy(BO_2)_3$, via normal-pressure synthesis, Z. Kristallogr. N. Cryst. Struct. 223 (2008) 177–178, https://doi.org/10.1524/ncrs.2008.0073.
[19] H. Emme, T. Nikelski, T. Schleid, R. Pöttgen, M.H. Möller, H. Huppertz, High-pressure synthesis, crystal structure, and properties of the new orthorhombic rare-earth *meta*-oxoborates $RE(BO_2)_3$ (RE = Dy–Lu), Z. Naturforsch. 59b (2004) 202–215, https://doi.org/10.1515/znb-2004-0213.
[20] H. Emme, G. Heymann, A. Haberer, H. Huppertz, High-pressure syntheses, crystal structures, and thermal behaviour of β-$RE(BO_2)_3$ (RE = Nd, Sm, Gd), Z. Naturforsch. 62b (2007) 765–770, https://doi.org/10.1515/znb-2007-0603.
[21] B. Fuchs, H. Huppertz, β-$Eu(BO_2)_3$ – a new member of the β-$RE(BO_2)_3$ (RE = Y, Nd, Sm, Gd–Lu) structure family, Z. Naturforsch. 74b (2019) 685–692, https://doi.org/10.1515/znb-2019-0117.
[22] B. Fuchs, R.O. Kindler, G. Heymann, H. Huppertz, High-pressure synthesis and crystal structure of the samarium *meta*-oxoborate γ-$Sm(BO_2)_3$, Z. Naturforsch. 75b (2020) 589–595, https://doi.org/10.1515/znb-2020-0045.
[23] G. Heymann, T. Soltner, H. Huppertz, δ-$La(BO_2)_3$ (≡ δ-LaB_3O_6): a new high-pressure modification of lanthanum *meta*-oxoborate, Solid State Sci. 8 (2006) 821–829, https://doi.org/10.1016/j.solidstatesciences.2006.03.002.
[24] A. Haberer, G. Heymann, H. Huppertz, High-pressure synthesis, crystal structure, and properties of δ-$Ce(BO_2)_3$, Z. Naturforsch. 62b (2007) 759–764, https://doi.org/10.1515/znb-2007-0602.
[25] A. Pitscheider, R. Kaindl, O. Oeckler, H. Huppertz, The crystal structure of π-$ErBO_3$: new single-crystal data for an old problem, J. Solid State Chem. 184 (2011) 149–153, https://doi.org/10.1016/j.jssc.2010.11.018.
[26] P. Chen, R.K. Li, Two high terbium content apatites: $Tb_5Si_2BO_{13}$ and $Tb_{4.66}Si_3O_{13}$, J. Alloys Compd. 622 (2015) 859–864, https://doi.org/10.1016/j.jallcom.2014.10.159.
[27] S. Bräuchle, H. Huppertz, Synthesis and structural characterization of the new rare-earth borosilicates $Pr_3BSi_2O_{10}$ and $Tb_3BSi_2O_{10}$, Z. Naturforsch. 70b (2015) 929–934.
[28] T.A. Teichtmeister, M.M. Hladik, H. Huppertz, High-pressure synthesis and crystal structure determination of $Tb_2SiB_2O_8$, Z. Naturforsch. 78b (2023) 25–31, https://doi.org/10.1515/znb-2022-0140.
[29] H. Huppertz, Multianvil high-pressure/high-temperature preparation, crystal structure, and properties of the new oxoborates $Dy_4B_6O_{14}(OH)_2$ and $Ho_4B_6O_{14}(OH)_2$, J. Solid State Chem. 177 (2004) 3700–3708, https://doi.org/10.1016/j.jssc.2004.06.026.
[30] M. Zoller, G. Heymann, A. Saxer, H. Huppertz, High-pressure synthesis of the acentric borate $DyB_5O_8(OH)_2$, Eur. J. Inorg. Chem. 2020 (2020) 370–376, https://doi.org/10.1002/ejic.201901285.
[31] S.C. Neumair, R. Kaindl, R.-D. Hoffmann, H. Huppertz, The new high-pressure borate hydrate $Cu_3B_6O_{12} \cdot H_2O$, Solid State Sci. 14 (2012) 229–235, https://doi.org/10.1016/j.solidstatesciences.2011.11.018.
[32] D. Walker, Lubrication, gasketing, and precision in multianvil experiments, Am. Mineral. 76 (1991) 1092–1100.
[33] H. Huppertz, Multianvil high-pressure/high-temperature synthesis in solid state chemistry, Z. Kristallogr. 219 (2004) 330–338.
[34] Bruker AXS Inc, SAINT, Bruker AXS Inc, Madison (WI), USA, 2021.
[35] Bruker AXS Inc, APEX4, Bruker AXS Inc, Madison (WI), USA, 2021.
[36] Bruker AXS GmBH, SADABS, Bruker AXS GmBH, Karlsruhe (Germany), 2016.
[37] L. Krause, R. Herbst-Irmer, G.M. Sheldrick, D. Stalke, Comparison of silver and molybdenum microfocus X-ray sources for single-crystal structure determination, J. Appl. Crystallogr. 48 (2015) 3–10, https://doi.org/10.1107/S1600576714022985.
[38] G.M. Sheldrick, Shelxt - integrated space group and crystal structure determination, Acta Crystallogr. A71 (2015) 3–8.
[39] Bruker AXS Inc, SHELXT - Crystal Structure Solution, Bruker AXS Inc, 2018.
[40] A.L. Spek, Single-crystal structure validation with the program PLATON, J. Appl. Crystallogr. 36 (2003) 7–13, https://doi.org/10.1107/S0021889802022112.
[41] A.L. Spek, Structure validation in chemical crystallography, Acta Crystallogr. D65 (2009) 148–155, https://doi.org/10.1107/S090744490804362X.
[42] A.L. Spek, Platon squeeze: a tool for the calculation of the disordered solvent contribution to the calculated structure factors, Acta Crystallogr. C71 (2015) 9–18, https://doi.org/10.1107/S2053229614024929.
[43] A.L. Spek, What makes a crystal structure report valid? Inorg. Chim. Acta. 470 (2018) 232–237, https://doi.org/10.1016/j.ica.2017.04.036.
[44] A.L. Spek, checkCIF validation ALERTS: what they mean and how to respond, Acta Crystallogr. E76 (2020) 1–11, https://doi.org/10.1107/S2056989019016244.
[45] G.M. Sheldrick, Crystal structure refinement with SHELXL, Acta Crystallogr. C71 (2015) 3–8, https://doi.org/10.1107/S2053229614024218.
[46] O.V. Dolomanov, L.J. Bourhis, R.J. Gildea, J.A.K. Howard, H. Puschmann, OLEX2 a complete structure solution, refinement and analysis program, J. Appl. Crystallogr. 42 (2009) 339–341, https://doi.org/10.1107/S0021889808042726.
[47] STOE, CIE GmbH, P. Stadi, The Rapid Comprehensive Modular System with Unsurpassed Reliability, STOE & CIE GmbH, 2018.
[48] B.-D. Dectris Ltd, Technical Documentation: MYTHEN Detector System, B.-D. Dectris Ltd, 2015.
[49] STOE & CIE GmbH, Accessories, STOE & CIE GmbH, Darmstadt (Germany), 2018.
[50] H.M. Rietveld, Line profiles of neutron powder-diffraction peaks for structure refinement, Acta Crystallogr. 22 (1967) 151–152, https://doi.org/10.1107/S0365110X67000234.
[51] D.K. Smith, J. Fiala, E. Ryba, Book reviews - the Rietveld method, Young R. A, Powder Diffr. 8 (1993) 252–254, https://doi.org/10.1017/S0885715600019497.
[52] A.X.S. Bruker, TOPAS: Total Pattern, Bruker AXS, Karlsruhe (Germany), 2009.
[53] S.K. Kurtz, T.T. Perry, A powder technique for the evaluation of nonlinear optical materials, J. Appl. Phys. 39 (1968) 3798–3813, https://doi.org/10.1063/1.1656857.
[54] Bruker Corporation, OPUS, Bruker Corporation, Billerica, MA, USA, 2012.
[55] R. Velchuri, B.V. Kumar, V.R. Devi, G. Prasad, D.J. Prakash, M. Vithal, Preparation and characterization of rare earth orthoborates, $LnBO_3$ (Ln = Tb, La, Pr, Nd, Sm, Eu, Gd, Dy, Y) and $LaBO_3$:Gd, Tb, Eu by metathesis reaction: ESR of $LaBO_3$:Gd and

luminescence of $LaBO_3$:Tb, Eu, Mater. Res. Bull. 46 (2011) 1219–1226, https://doi.org/10.1016/j.materresbull.2011.04.006.
[56] C.T. Prewitt, R.T. Downs, High-pressure crystal chemistry, Rev. Mineral. Geochem. 37 (1998) 284–318.
[57] E. Zobetz, Geometrische Größen und einfache Modellrechnungen für BO_4 -Gruppen, Z. Kristallogr. 191 (1990) 45–57, https://doi.org/10.1524/zkri.1990.191.1-2.45.
[58] N.E. Brese, M. O'Keeffe, Bond-valence parameters for solids, Acta Crystallogr. B47 (1991) 192–197, https://doi.org/10.1107/S0108768190011041.
[59] M. Nespolo, B. Guillot, CHARDI2015 charge distribution analysis of non-molecular structures, J. Appl. Crystallogr. 49 (2016) 317–321, https://doi.org/10.1107/S1600576715024814.
[60] T. Steiner, The hydrogen bond in the solid state, Angew. Chem. Int. Ed. 41 (2002) 48–76, https://doi.org/10.1002/1521-3773(20020104)41:1<48:AID-ANIE48>3.0.CO;2-U.
[61] V.G. Dmitriev, D.N. Nikogosyan, Effective nonlinearity coefficients for three-wave interactions in biaxial crystal of mm2 point group symmetry, Opt Commun. 95 (1993) 173–182, https://doi.org/10.1016/0030-4018(93)90066-E.
[62] D.A. Kleinman, Nonlinear dielectric polarization in optical media, Phys. Rev. 126 (1962) 1977, https://doi.org/10.1103/PhysRev.126.1977. –1979.
[63] K. Nakamoto, M. Margoshes, R.E. Rundle, Stretching frequencies as a function of distances in hydrogen bonds, J. Am. Chem. Soc. (1955) 6480–6486.
[64] S.D. Ross, The vibrational spectra of some minerals containing tetrahedrally co-ordinated boron, Spectrochim. Acta (1972) 1555–1561.
[65] R. Kaindl, G. Sohr, H. Huppertz, Experimental determinations and quantum-chemical calculations of the vibrational spectra of β-ZnB_4O_7 and β-CaB_4O_7, Spectrochim. Acta, Part A 116 (2013) 408–417, https://doi.org/10.1016/j.saa.2013.07.072.
[66] H. Huppertz, B. von der Eltz, Multianvil high-pressure synthesis of $Dy_4B_6O_{15}$: the first oxoborate with edge-sharing BO_4 tetrahedra, J. Am. Chem. Soc. 124 (2002) 9376–9377, https://doi.org/10.1021/ja017691z.
[67] J. Lin, D. Sheptyakov, Y. Wang, P. Allenspach, Structures and phase transition of vaterite-type rare earth orthoborates: a neutron diffraction study, Chem. Mater. 16 (2004) 2418–2424, https://doi.org/10.1021/cm0499388.
[68] P. Mukherjee, Y. Wu, G.I. Lampronti, S.E. Dutton, Magnetic properties of monoclinic lanthanide orthoborates, $LnBO_3$, Ln = Gd, Tb, Dy, Ho, Er, Yb, Mater. Res. Bull. 98 (2018) 173–179, https://doi.org/10.1016/j.materresbull.2017.10.007.